Rev.Adv.Mater.Sci. 15(2007) 150-157

SELF-ORGANIZATION AND OPTICAL RESPONSE OF SILVER NANOPARTICLES DISPERSED IN A DIELECTRIC MATRIX

D. Lantiat, J. Toudert, D. Babonneau, S. Camelio, C. Tromas and L. Simonot

Laboratoire de Métallurgie Physique, UMR 6630 CNRS, Université de Poitiers, SP2MI, Téléport 2, Bvd M. & P. Curie, BP 30179, 86962 Futuroscope Chasseneuil Cedex, France

Received: January 22, 2007

Abstract. Double ion-beam sputtering has been used to fabricate nanocermet multilayers consisting of silver nanoparticles sandwiched between Si_3N_4 dielectric layers. The organization of the nanoparticles has been studied in detail by quantitative analysis of transmission electronic microscopy and atomic force microscopy images. Our results show that the nanoparticles deposited on a plane surface present an isotropic macroscopic in-plane organization while their vertical arrangement displays a topology-induced self-organization. The use of faceted alumina substrates with periodic hill-and-valley structures results in the formation of linear chains of silver particles along the valleys. In that case, transmission optical measurements reveal in-plane anisotropy.

1. INTRODUCTION

Because of their reduced size, metallic nanoparticles have specific properties, different from those of the bulk materials, which have been shown to depend not only on the morphology of the nanoparticles (shape, size) but also on their spatial organization [1,2]. For example, the optical response of nanocermets thin films, consisting of nanoparticles embedded in a transparent dielectric matrix, is characterized by a surface plasmon resonance (SPR) which results in an absorption band [2] located in the visible spectral region for noble metals. In previous papers [3-5], we have shown that the shape and the size of silver particles embedded in a Si_3N_4 matrix produced by ion-beam sputtering can be tailored by adjusting the parameters of the fabrication process. As a consequence, the position of the SPR wavelength can be controlled from 400 nm to 700 nm. Recently, it has also been reported that faceted substrates can be used to produce ordered arrays of metallic nanoparticles chains with anisotropic optical or magnetic properties [6-10]. In this paper, we focus on the structural study of silver nanoparticles sandwiched between Si_3N_4 dielectric layers deposited onto plane and nanostructured surfaces. We show that quantitative analysis of transmission electron microscopy (TEM) and atomic force microscopy (AFM) images can be performed to investigate in detail the spatial organization of the nanoparticles. Finally, the effects of self-organization on the optical properties of the nanocermets are discussed.

2. EXPERIMENTAL DETAILS

$[Si_3N_4(t_{buffer})/Ag(t_{Ag})]_N/ Si_3N_4(t_{cap})$ multilayers (with t_{buffer}, t_{Ag}, t_{cap} and N being the buffer thickness, the silver-layer thickness, the cap thickness and the number of silver layers, respectively) were grown

Corresponding author: D. Lantiat , e-mail: david.lantiat.baillargue@etu.univ-poitiers.fr

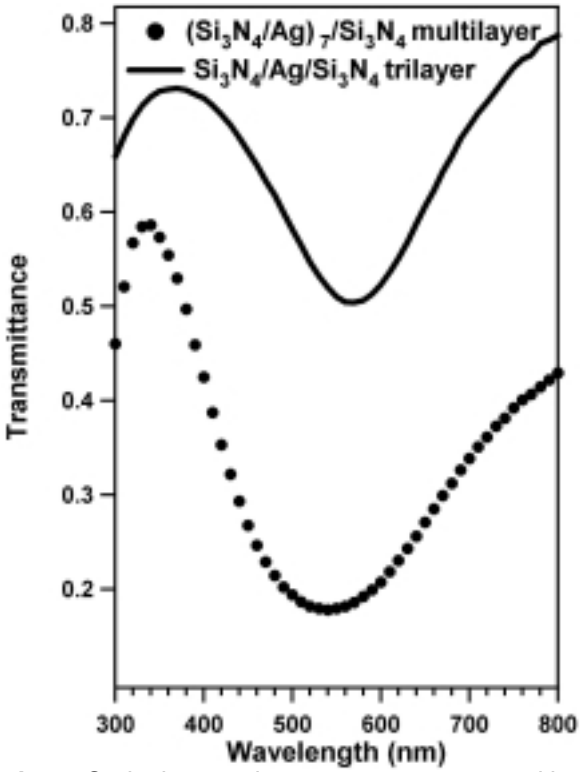

Fig. 1. Optical transmittance spectra at normal incidence of a $Si_3N_4/Ag/Si_3N_4$ trilayer (t_{buffer}=15 nm, t_{Ag}=1 nm, t_{cap}=15 nm) and a $(Si_3N_4/Ag)_7$ multilayer (t_{buffer}=12 nm, t_{Ag}=1 nm, t_{cap}=12 nm) deposited on fused silica.

at 200 °C by double ion-beam sputtering in a Nordiko 3000 chamber. Argon ions (energy 1200 eV, current 80 mA) were used to sputter alternatively a Si_3N_4 target and a silver target mounted on a rotative holder. A secondary nitrogen-ion beam (energy 50 eV, current 40 mA) was used to bombard the films during the deposition of the dielectric material in order to obtain the Si:N stoichiometry. The deposition sequence always started and finished with a Si_3N_4 layer so that Ag nanoparticles nucleate always on the same type of surface and are protected against atmospheric contamination. The sputtered species were deposited onto different substrates: surface oxidized Si(001), carbon-coated copper grids, fused silica, plane and faceted Al_2O_3(0001) with nominal inclined angle of 3°.

Morphology and organization of the nanoparticles were investigated from in-plane and cross-section views by TEM performed with a JEOL 200CX microscope operated at 200 kV. Direct observations of the surface of the multilayers were carried out by AFM with a Nanoscope Digital instrument. The optical properties were investigated by transmittance measurement at normal incidence between 210 and 900 nm with a 5 nm monochromator step. As typical example, Fig. 1 shows the transmittance spectra of a $Si_3N_4/Ag/Si_3N_4$ trilayer (t_{buffer}=15 nm, t_{Ag}=1 nm, t_{cap}=15 nm) and a $(Si_3N_4/Ag)_7$ multilayer (t_{buffer}=12 nm, t_{Ag}=1 nm, t_{cap}=12 nm) deposited on fused silica. Each sample displays a SPR at 570 nm and 540 nm, respectively, consistent with the presence of metallic nanoparticles. This difference can be interpreted in term of interaction due to organization effects [4], which are investigated in details in this paper.

3. RESULTS AND DISCUSSION

3.1. In-plane organization in a $Si_3N_4/Ag/Si_3N_4$ trilayer

Fig. 2a exhibits a plane-view TEM micrograph of the $Si_3N_4/Ag/Si_3N_4$ trilayer (t_{buffer}=15 nm, t_{Ag}=1 nm, t_{cap}=15 nm) after numerical treatment. This treatment consists in applying a median filter to reduce noise in the image and a Wallis filter that adjusts brightness values in local areas by a locally-adaptive contrast enhancement [11]. This filtered plane-view TEM image gives an illustration of the trilayer structure, where a polydisperse assembly of dark nanometric particles is observed within a bright-contrast matrix. Fig. 2b shows the binarized image obtained from the filtered one, which enables to determine the particle density d=6168 μm^{-2}, the coverage rate τ = 22%, the mean particle diameter $<D>$=6.8 nm and the full-width at half-maximum of the D distribution w=4.2 nm [5]. It is worth noting here that a perfect thresholding is not realizable because if a threshold value is determined in order to respect the size of the biggest particles, the smallest ones will appear with a size lower than reality, and the smallest of them will disappear. However, we can estimate that the error on d and $<D>$ due to this process does not exceed ±10% [12].

In order to realize a quantitative study of the spatial organization of the particles, the binary image in Fig. 2b has been divided into nine 100×100 nm^2 cells and the autocorrelation function (ACF) of each cell has been calculated in Fig. 2c. The presence of intensity maxima in these local ACFs suggests that an in-plane short-range order exists between the Ag nanoparticles [13]. However, the averaged ACF presented in Fig. 2d is radially symmetric (annular form) showing that the macroscopic

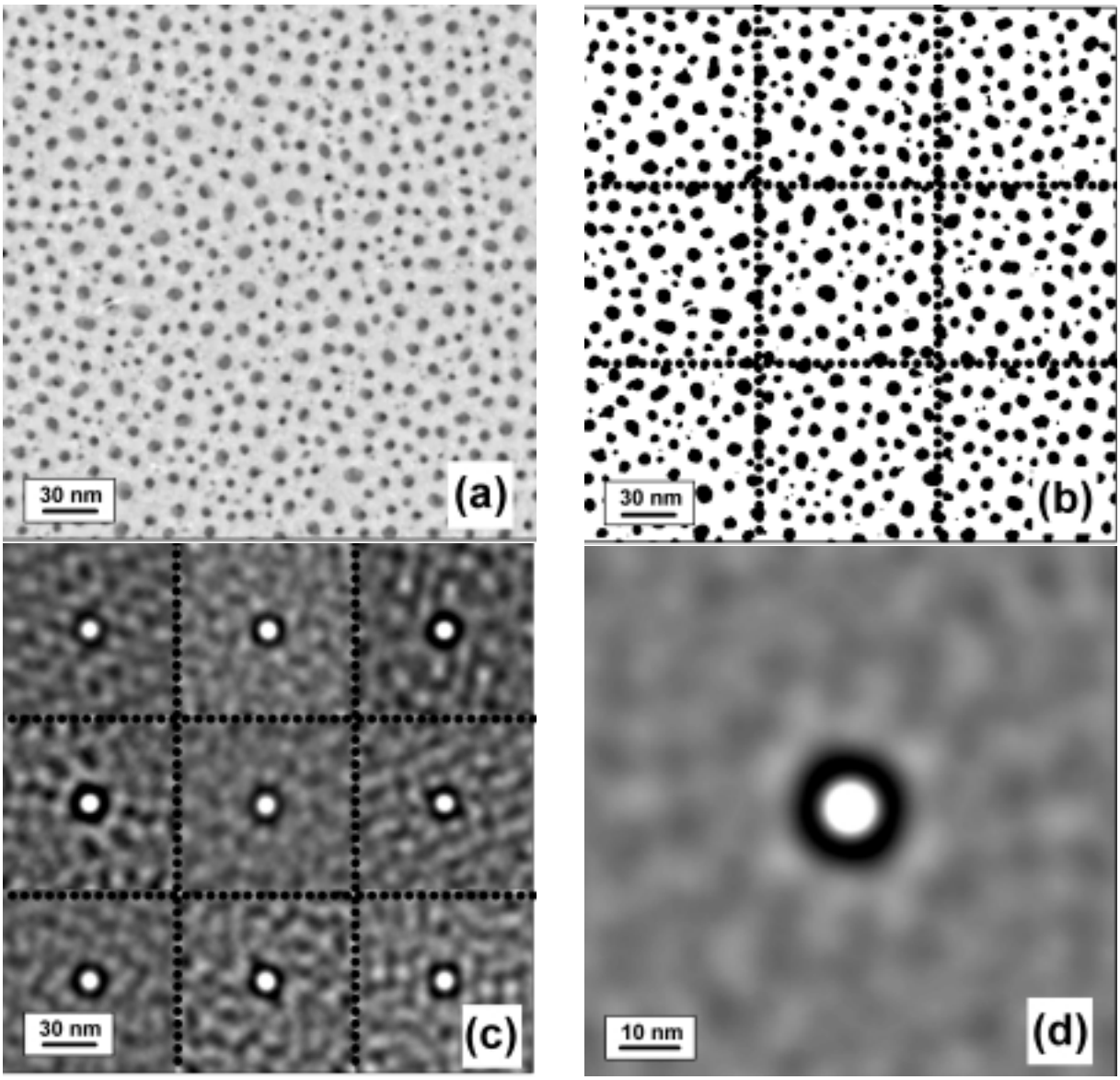

Fig. 2. (a) Filtered plane-view TEM image of a Si_3N_4/Ag/Si_3N_4 trilayer (t_{buffer}=15 nm, t_{Ag}=1 nm, t_{cap}=15 nm) deposited on carbon-coated copper grid. (b) Binarized image divided into nine 100×100 nm^2 cells. (c) Local autocorrelation functions. (d) Averaged autocorrelation function.

in-plane organization is isotropic without long-range order. In addition, from the radial profile of the averaged ACF, it is possible to determine the mean interparticle distance Λ_x=14.8 nm corresponding to the radius of the ring.

3.2. Vertical organization in a Si_3N_4/Ag multilayer

Under the same conditions as the trilayer, a (Si_3N_4/Ag)$_7$ (t_{buffer}=12 nm, t_{Ag}=1 nm, t_{cap}=12 nm) multilayer has been elaborated by fixing the number of Si_3N_4/Ag bilayers in order to obtain a total thickness around 100 nm. As for the detailed analysis of the plane-view TEM micrograph trilayer in part 3.1, the cross-section TEM micrograph (not shown) of the multilayer has been filtered, binarized, and divided into 100×100 nm^2 cells. Figs. 3a and 3b show a representative 100×100 nm^2 cell after filtering and thresholding treatment, respectively. The local ACF has been then calculated in Fig. 3c and the ACF

Table 1. Parameters used for the simulation of the averaged ACF of the $(Si_3N_4/Ag)_7$ multilayer: in-plane diameter D, height H, in-plane interparticle distance Λ_x, bilayer thickness Λ_z, and corresponding standard deviations δD, δH, $\delta\Lambda_x$, and $\delta\Lambda_z$.

$D\pm\delta D$ (nm)	$H\pm\delta H$ (nm)	$\Lambda_x\pm\delta\Lambda_x$ (nm)	$\Lambda_z\pm\delta\Lambda_z$ (nm)
7.7±1.2	4.4±0.4	12.6±2.6	13.5±0.1

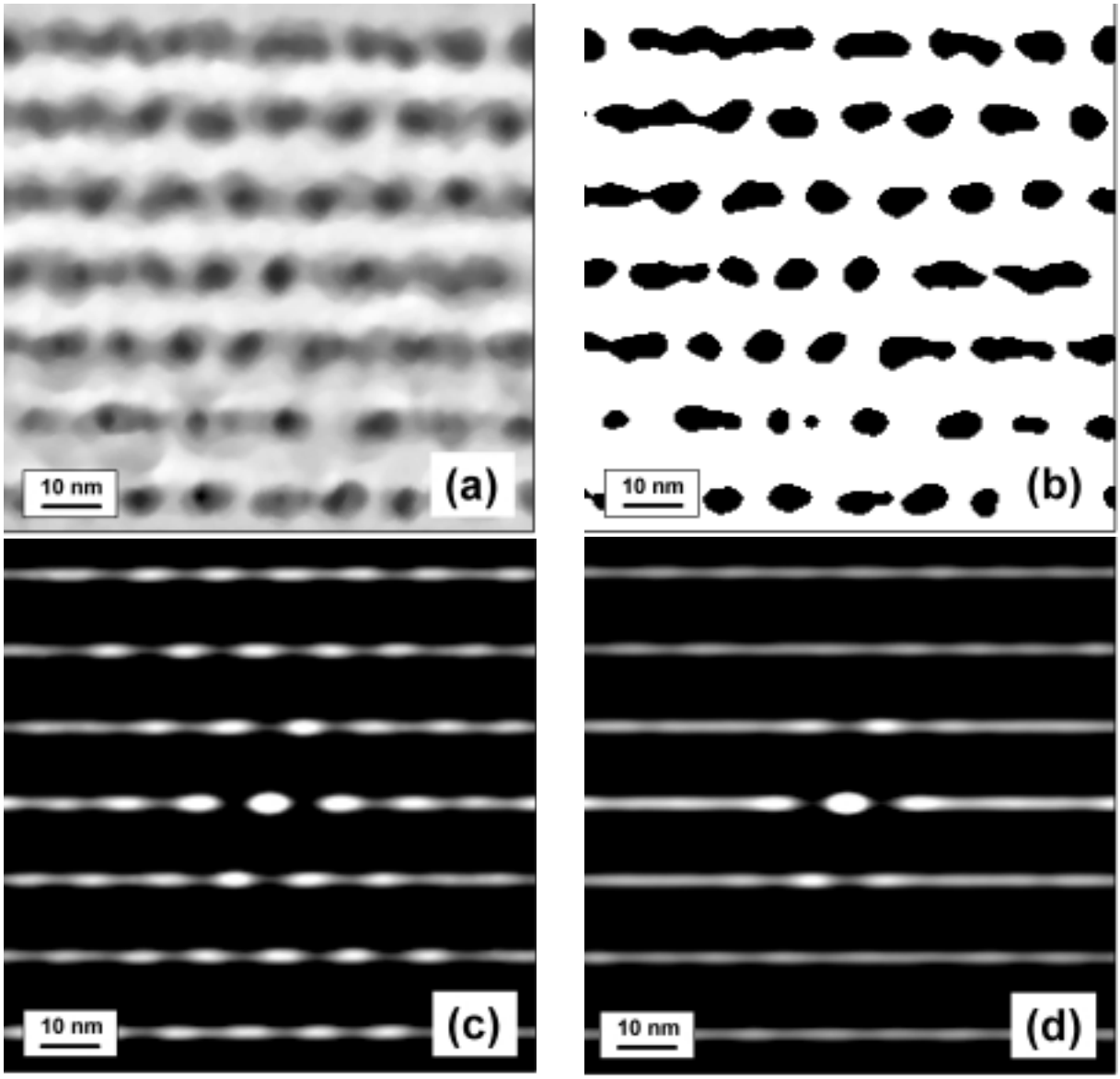

Fig. 3. (a) 100×100 nm^2 filtered cross-section TEM view cell of a $(Si_3N_4/Ag)_7$ multilayer (t_{buffer}=12 nm, t_{Ag}=1 nm, t_{cap}=12 nm) deposited on silicon. (b) Binarized image of the 100×100 nm^2 cell. (c) Autocorrelation function of the cell. (d) Averaged autocorrelation function over eight 100×100 nm^2 cells.

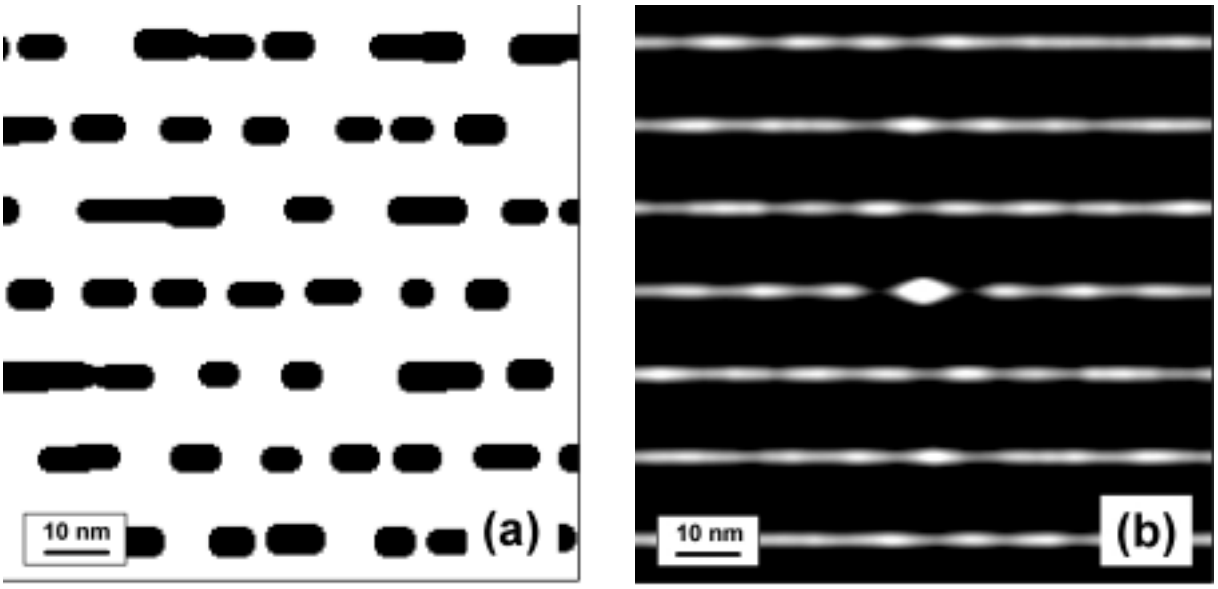

Fig. 4. (a) Simulated array of the Si_3N_4/Ag multilayer using the parameters gathered in Table 1. (b) Auto-correlation function of the simulated array.

averaged over eight cells, which returns account of the organization of the particles not only within each layer but also from layer to layer, is shown in Fig. 3d. Contrary to the trilayer case in Fig. 2d, secondary intensity maxima appear both in the local and in the averaged ACFs of the multilayer suggesting that the particles are organized vertically by adopting a hexagonal symmetry, as already observed in a Co/Al_2O_3 system [14]. From the position of the first secondary maxima, it is possible to estimate the mean in-plane interparticle distance within the Ag layer, Λ_x=12.5 nm, and the mean layer-to-layer distance, Λ_z=13.6 nm. It can be seen that the mean in-plane interparticle distance is slightly smaller than that of the trilayer containing similar amount of silver, which is most likely due to projection effects inherent to TEM observations. Furthermore, although the silver layers are discontinuous, the mean layer-to-layer distance is close to the expected value of 13 nm, i.e. to the nominal period of the multilayer. The projection effects do not allow reliable image analysis and it has been therefore necessary to perform numerical simulations of the averaged ACF to quantify the ordering of the particles within the multilayer. The procedure consists in comparing the ACF of a simulated particle array to that of the multilayer. To create the simulated particle array, we first consider particles with diameter *D* and height *H* arranged in a perfect centered-rectangular lattice with parameters Λ_x and Λ_z. Then we introduce for each particle a deviation from the initial size and position by assuming standard deviations δD, δH, $\delta\Lambda_x$, and $\delta\Lambda_z$. Finally, we calculate the ACF of the simulated array and the corresponding signal error defined as $\chi = [ACF_{exp}(x,y)-ACF_{sim}(x,y)]^2/ACF_{sim}(x,y)$. Fig. 4(a) shows the particle array simulated by using the parameters gathered in Table 1, which enables to minimize χ. It can be seen that the corresponding simulated ACF [Fig. 4b] reproduces satisfactorily the experimental ACF [Fig. 3d]. As expected, the $\delta\Lambda_z$ value is found to be very weak ($\delta\Lambda_z/\Lambda_z$=0.7%) owing to the deposition method, which consists in depositing alternatively and periodically the Si_3N_4 and Ag layers. In addition it is worth noting that, although higher than the $\delta\Lambda_z$ value, the $\delta\Lambda_x$ value is also rather weak ($d\Lambda_x/\Lambda_x$=20.6%). From our simulations, we are able to determine the mean height *H* and the mean diameter *D* of the silver nanoparticles. It should be however noted that whereas the *H* value of 4.4 nm is significant since the Ag layers are well separated, the *D* value of 7.7 nm is probably over-estimated due to projection effects. Accordingly, the $\delta\Lambda_x/\Lambda_x$ value of 20.6%

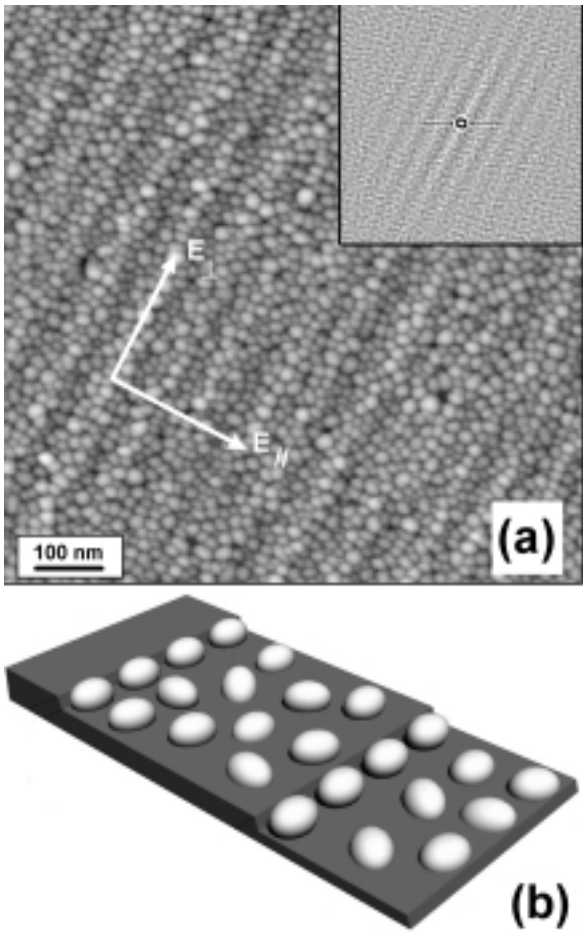

Fig. 5. Filtered AFM image of a $Si_3N_4/Ag/Si_3N_4$ trilayer (t_{buffer}=1 nm, t_{Ag}=2 nm, t_{cap}=12 nm) deposited on 3° inclined faceted alumina substrate and the corresponding autocorrelation function (inset). (b) Schematic of the nanoparticles arrangement after silver deposition.

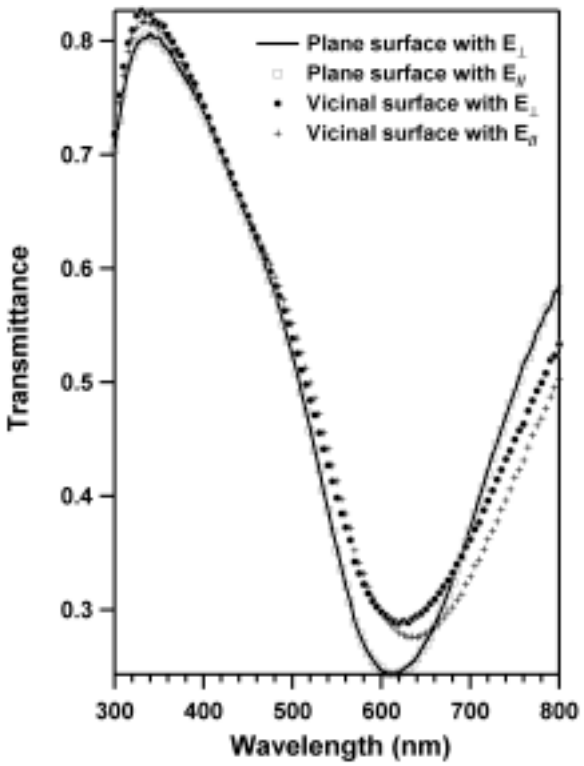

Fig. 6. Optical transmittance spectra at normal incidence of $Si_3N_4/Ag/Si_3N_4$ trilayers (t_{buffer}=1 nm, t_{Ag}=2 nm, t_{cap}=12 nm) deposited on Al_2O_3(0001) substrates with nominal inclined angles of 0° and 3° for light polarizations parallel and perpendicular to the facets.

is also over-estimated attesting to the self-organized growth of the Ag nanoparticles.

Actually, the origin of the self-organization may be related to the topology of the Si_3N_4 capping layers, which are corrugated and present a hill-and-valley structure on a mesoscopic scale as previously observed in $Si_3N_4/Ag/Si_3N_4$ trilayers [5,15]. This result suggests that there is a preferential nucleation of the particles of the n^{th} Ag layer in the valleys of the Si_3N_4 layer covering the $(n\text{-}1)^{th}$ Ag layer. Thus, each new Ag layer is organized with a "memory effect" of the organization of the subjacent layers. Accordingly, in-plane self-organization would be expected in $Si_3N_4/Ag/Si_3N_4$ trilayers deposited onto surfaces with periodic hill-and-valley structures.

3.3. In-plane self-organization with nanostructured surfaces

Faceted Al_2O_3(0001) substrate with nominal inclined angle of 3° has been used as nanoscale template in order to produce an in-plane self-organization of silver nanoparticles. Such a substrate presents a "hill-and-valley" profile with average terraces width of 80 nm and step height of 5 nm, respectively. Fig. 5a exhibits the filtered AFM image and its ACF (inset) of a 3° inclined alumina substrate covered by a $Si_3N_4/Ag/Si_3N_4$ trilayer (t_{buffer}=1 nm, t_{Ag}=2 nm, t_{cap}=12 nm). A schematic of the nanoparticles arrangement after silver deposition is also shown in Fig. 5b. The buffer thickness has been reduced to 1 nm to prevent smoothing of the

substrate topography. A simple inspection of the image suggests that the surface topography is indeed preserved after the deposition of the trilayer and that the macroscopic in-plane organization of the nanoparticles is anisotropic.

More precisely, the detailed analysis of the ACF reveals (i) a slightly elliptic central ring (long axis *a* = 25.3 nm and short axis *b* = 23.9 nm respectively perpendicular and parallel to the steps) corresponding to the quasi-isotropic nucleation of Ag particles and (ii) lines oriented parallel to the steps corresponding to the formation of self-organized chains of nanoparticles with a mean interchain distance $\Lambda_{\perp}$=80 nm in excellent agreement with the average terrace width. On such faceted templates, the nucleation is possible on terraces [16] or along the steps [6]. The self-organization of nanoparticles on terraces has been already observed by Okamoto *et al.* in the case of FePt nanoparticles grown on MgO(110) with groove structure [16]. The authors proposed that the self-organization is due to a geometrical limitation of the particle growth along the cross-groove direction as the particle size approaches the groove width. In our case, the size of the Ag particles is much smaller than the width of the terraces so that the growth mechanism proposed by Okamoto *et al.* is unlikely. Consequently, and according to the results presented in part 3.2, the self-organized particle chains must be situated along the steps, which are preferential nucleation sites because of their increased coordination number with respect to that of the terrace width [6].

Fig. 6 shows the transmittance spectra at normal incidence of the same Si_3N_4/Ag/Si_3N_4 trilayer deposited onto plane and 3° inclined alumina substrates obtained for two perpendicular directions of the incident electric field. For the trilayer deposited onto the plane alumina substrate, the SPR is centered around 620 nm whatever the direction of the field in the plane. This result confirms that the macroscopic in-plane organization of the nanoparticles deposited on a plane surface is isotropic. In contrast, the SPRs for the trilayer deposited onto the 3° inclined alumina substrate are centered at 640 nm and 620 nm for polarizations parallel and perpendicular to the steps respectively. It is worth noting in Fig. 5 that a certain fraction of silver particles stick together to form linear chains of finite size in the direction parallel to the surface steps. Consequently a dipole-dipole coupling among neighbouring particles is probably responsible for the splitting of the SPR [6]. Indeed these interactions can be taken into account by a set of effective depolarization factors which are fictitious quantities (not related to any ellipsoidal shape) but that acts formally as a shape effect [1]. However, the fraction of silver particles onto terraces is high compared to those of particles chains, as schematized in Fig. 5b. These terrace particles behave as independent particles with an isotropic optical contribution, which could explain the low value of this shift.

4. CONCLUSION

We have investigated by TEM and AFM the spatial organization of silver nanoparticles sandwiched between Si_3N_4 layers. From the detailed analysis of local and averaged ACFs, we show that the nanoparticles deposited on a plane surface are organized in an isotropic way and present an order at short distance. In contrast, the nanoparticles deposited on corrugated or faceted surfaces nucleate preferentially in the hollows formed by the Si_3N_4 capping layers. This leads to the vertical self-organization of the nanoparticles in Si_3N_4/Ag multilayers and to the formation of chains of nanoparticles in Si_3N_4/Ag/Si_3N_4 trilayers deposited onto faceted alumina. In this case, transmission optical measurements reveal in-plane anisotropy with a splitting of the longitudinal and transverse SPRs attributed to a dipole-dipole coupling (or even higher multipole effect) among particles chains.

ACKNOWLEDGEMENTS

We thank P. Guérin for his help during the preparation of the nanocomposites and M.-F. Denanot for performing the TEM observations.

REFERENCES

[1] C.G. Granqvist and O.Hunderi // *Phys. Rev. B* **16** (1977) 3513.

[2] U.Kreibig and M.Vollmer, *Optical Properties of Metal Particles* (Springer, Berlin, 1995).

[3] S.Camelio, D.Babonneau, T.Girardeau, J.Toudert, F.Lignou, M.-F.Denanot, N.Maître, A.Barranco and P.Guérin // *Appl. Opt.* **42** (2002) 674.

[4] T.Girardeau, S.Camelio, D.Babonneau, J.Toudert and A.Barranco // *Thin Solid Films* **455-456** (2004) 313.

[5] J.Toudert, S.Camelio, D.Babonneau, M.-F.Denanot, T.Girardeau, J.P.Espinos, F.Yubero and A.R.Gonzalez-Elipe // J. *App. Phys.* **98** (2005) 114316/1.

[6] E.Fort, C.Ricolleau and J.Sau-Pueyo // *Nanoletters* **3** (2003) 65.
[7] T.Kitahara, A.Sugawara, H.Sano and G.Mizutani // *Appl. Surf. Sci.* **219** (2003) 271.
[8] A.Sugawara, G. G. Hembree and M. R. Scheinfein // *J. Appl. Phys.* **82** (1997) 5662.
[9] J. Oster, M. Kallmayer, L. Wiehl, H. J. Elmers, H. Adrian, F. Porrati and M. Huth // *J. Appl. Phys.* **97** (2005) 014303.
[10] C. Teichert // *Appl. Phys. A:Mater. Sci. Process.* **76** (2003) 653.
[11] W.K. Pratt, *Digital Image Processing 2nd edition United States of America* (John Wiley & Sons INC, 1991).
[12] J.Carrey, J.-L.Maurice, F.Petroff and A.Vaurčs // *Surf. Sci.* **504** (2002) 75.
[13] D.Babonneau, F.Pailloux, J.-P.Eymery, M.-F.Denanot and P. Guérin // *Phys. Rev. B* **71** (2005) 035430/1.
[14] D.Babonneau, F.Petroff, J.-L.Maurice, F.Fettar and A.Vaurès // *Appl. Phys. Lett.* **76** (2000) 2892.
[15] S.Camelio, J.Toudert, D.Babonneau and T.Girardeau // *Appl. Phys. B* **80** (2004) 89.
[16] S.Okamoto, O.Kitakami, T.Miyazaki, Y.Shimada, Y.K.Takahashi and K.Hono // *J. App. Phys.* **96** (2004) 5217.